GUST EFFECT FACTORS OF COMPONENTS AND CLADDING WIND LOADS FOR LOW-SLOPE ROOFS ON LOW-RISE BUILDINGS

Jigar Mokani[1][0000-0002-9810-3555] and Jin Wang [2,3] [0000-0001-9536-6432]

[1] M.E.Sc. student, Department of Civil & Environment Engineering, University of Western Ontario, Canada, N6A 5B9
[2] Assistant professor, Department of Civil & Environment Engineering, University of Western Ontario, Canada, N6A 5B9
[3] jwan2225@uwo.ca

Abstract. Building Components and Cladding (C&C) are important to the performance of these structures during extreme windstorms. Post-damage surveys have revealed that low-rise building roofs are particularly vulnerable to windstorms. Therefore, accurate prediction of wind loads on C&C of low-rise building roofs is essential to increase building resilience and mitigate the risks of damage to these structures. The gust effect factor method, developed based on Quasi-steady Theory (QST), has been widely used to determine design wind loads in many codes of practice, primarily for the along-wind overall response of high-rise buildings. The present study examines the applicability of gust effect factor method for predicting C&C wind loads of low-rise building roofs. The flow fields over roofs are relatively complex, with many types of flow patterns and vortical structures that might alter the Gaussian statistics. One building configuration from the NIST database obtained from Boundary-Layer Wind Tunnel II at the University of Western Ontario was used to conduct the analysis. The skewness and kurtosis of C&C wind loads were examined first to demonstrate the statistical distributions of C&C wind load on low-rise building roofs. In addition, the gust effect factors, which relate the wind load fluctuations to upstream wind turbulence, were presented. The results show that the gust effect factors of wind loads on roof corner zones extend the recommended value of 0.85 in ASCE 7-22 due to the complicated conical vortices. Furthermore, it is observed that the gust effect factors vary with effective wind area in the same way as peak wind pressures suggested in ASCE 7-22 and NBCC 2020. This study highlights that the gust effect factor method can be reasonable for predicting C&C wind loads for large effective wind area. However, it may underestimate peak wind loads due to the neglect of body-generated turbulence.

Keywords: Gust effect factors, Components and Cladding, Low-rise buildings, Quasi-steady theory.

1 Introduction

Low-rise buildings are typically used for residential, commercial or industrial purposes, and their lateral force resisting systems are usually designed for wind actions rather than seismic activities [1]. In North America, the majority of low-rise buildings are

constructed using light-framed wood. However, these light-framed buildings are susceptible to significant damage during strong windstorms, resulting in considerable economic loss, injuries, and sometimes fatalities [2]. For instance, the damage caused by hurricane Katrina in 2005 was estimated to be nearly USD 108 billion, making it one of the costliest natural disaster in US history. Similarly, Super typhoon Yolanda in 2013 caused USD 2.9 billion in damage in south-east Asia [3]. The Institute of Business & Home Safety (IBHS) indicated in its hurricane Ike & Charley report that roofs had the highest failure rate out of all building components [4]. Moreover, it has been observed that roof components, such as sheathing and covering, are particularly vulnerable to severe damage, which can be hazardous. Post-disaster surveys have provided evidence that failure of roof coverings accounts for much of initial damage [5]. Therefore, there is a significant need to accurately estimate the wind loads on Components & Cladding (C&C) of building roofs to increase the resilience of low-rise buildings and mitigate the risks of damage to these structures.

The design wind loads in building codes/standards, such as ASCE 7-22 [6] and NBCC 2020 [7], are typically determined using two methods. The first is the gust effect factor approach, which was firstly proposed by Davenport [8] and initially named as gust response factor. Later on, Solari [9][10] related this gust response factor into gust velocity based on Quasi-steady theory, and further developed the gust effect factor model with a closed solution. This gust effect factor method considers both background turbulence effects and resonant dynamic effects and was primarily developed for overall along-wind response of high-rise buildings. However, for rigid buildings, such as low-rise buildings, ASCE 7-22 suggests to use a constant gust effect factor value of 0.85. The second method for determining design wind loads is based on directly measured peak wind pressures, which is commonly used for C&C wind loads in both ASCE 7-22 and NBCC 2020. There are differences in the C&C wind load provisions between ASCE 7-22 and NBCC 2020. Previously, the wind load provisions for C&C in NBCC 2020 and earlier versions of ASCE 7-16 [16] were largely based on the work of Stathopoulos [11], supplemented by Meecham [12] for hip roofs, and were updated by Stathopoulos et al. [13]. However, Kopp & Morrison [5] revised the wind loads for C&C of low-rise building with low-sloped gable roof, which have been adopted in ASCE 7-16 and later versions.

Given the two methods for determining design wind loads, one would like to know if the gust effect factor method can be applied for estimating C&C wind loads, or to what extent this method can be used. However, there has been no investigation of gust effect factors for C&C wind loads on low-rise building roofs, which is the primary motivation of this study. To determine whether the gust effect factor method is suitable for estimating C&C wind loads, it is necessary to examine the assumptions that underlie the concept. There are two implicit assumptions in gust effect factor concept: (i) Gaussian distribution of wind loads, and (ii) negligible body-generated turbulence. Studies have indicated that the flow patterns around building roofs are relatively complex. For the flow past any building edge, a shear layer is formed by the flow separation. If the building surface is long enough, the separated shear layer will reattach downstream (i.e., impinge on the surface), forming a separation bubble. The separated shear layer and

separation bubble have several instabilities associated with them, which control the nature of the vortices shedding and/or advecting downstream. While for oblique wind directions, the conical vortices are observed and responsible for the peak suction near the leading edge or the corner of roofs [24]. These complicated vortical structures and associated body-generated turbulence may conflict with the assumptions in QST [9][10]. For example, Wang and Kopp [25] found that the separated flow without reattachment on building surfaces would lead the wind loads to follow non-Gaussian distribution with large skewness and kurtosis. However, Wu and Kopp [14] found that the QST still holds for building roofs with large areas. Based on this, a reasonable hypothesis is that gust effect factor concept is applicable for large areas on building roofs but may lose accuracy for small areas.

The objective of this paper is to examine the applicability of the gust effect factor (G) of C&C wind loads on the roof of a selected low-rise building. Specifically, this study focuses on one building configuration from the NIST database. Section 2 of this paper outlines the methodology adopted to determine the gust effect factor, as well as other statistical parameters. In Section 3, zone-wise aerodynamic results related to gust effect factor and statistical characteristics, such as skewness and kurtosis, are presented. Section 4 summarized the findings and discuss the potential for future research in this area.

2 Methodology for Estimating Statistical Parameters

2.1 Dataset used in the present study

For the presented research, a low-rise building with a 1:12 roof slope was selected from NIST database. The building dimensions are 125' × 80' × 40' (length × width × eave-height), and an isometric view and tap layout can be seen in Fig.1. A total of 336 taps were used to capture wind pressure distributions on the roof, with a high density of taps on one part of the roof. In this study, we divide the roof into three different zones as defined in NBCC 2020 [7], as shown in Fig. 2. However, note that ASCE 7-22 has different definitions in terms of zone size and location. Four corner zones (Zone A-1 to A-4) were defined as 10% of the least horizontal dimension or 0.4H (where H is eave height), whichever is smaller but not less than 4% of the least dimension or 1m, as per NBCC 2020 [7]. Edge zones (Zone B-1 to B-4) were defined with the same width as the corner zones and extended between the corner zones, while the remaining central region was defined as the interior zone (Zone C), as shown in Fig. 2. The wind direction is also indicated in Fig. 2.

The wind tunnel test utilized a 1:100 scale model for this building for open and suburban terrains [15]. The wind direction was sampled every 5° from 180° to 360°, and the sampling rate was 500 Hz for a period of 100 s. The pressure data at each tap location were referenced to the dynamic velocity pressure measured at a higher level in the wind tunnel, where the flow is uniform with low turbulence level. To obtain the pressure data referenced at mean roof height, all the data needed to be re-referenced to the mean roof height dynamic pressure by the ratio of dynamic pressure at the upper level and the dynamic pressure at mean roof height. More details on the experimental setup, such as

the pressure tap layout and wind simulation, can be found in Ho et al. [15]. In this study, we primarily focused on the pressure data for open terrain.

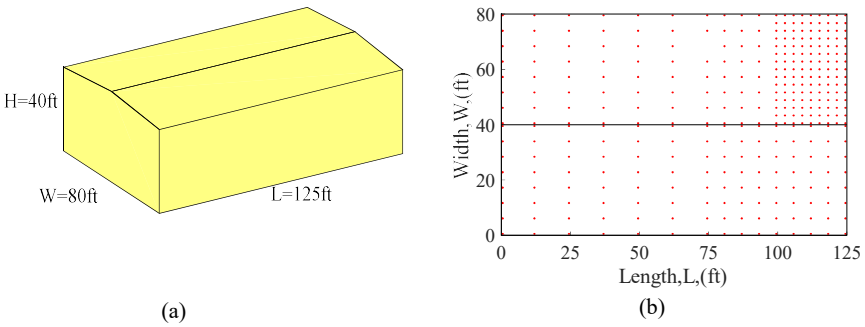

Fig. 1. Building configuration of this study: (a) Isometric view of building; (b) Tap layout on roof (the red dots indicate the pressure taps).

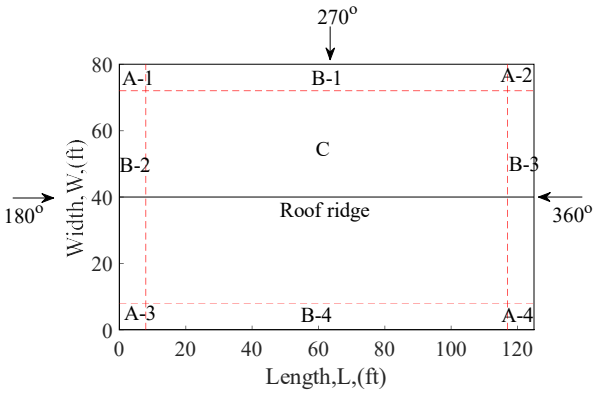

Fig. 2. Zone demarcation

2.2 Methodology in the present study

Aerodynamic pressures acting on structures fluctuate in both time and space domains, which means that the pressure differs from point to point. As the distance between two sample points increases, the spatial coherence of the pressures decreases [16], resulting in a reduction of peak wind loads on large tributary areas. As discussed in the previous section, the tap resolution on the roof is non-uniform. To reduce the effects of non-uniformly distributed taps, a mesh grid was created with 1 ft spacing along the length and width of the roof. The pressure assigned to the mesh grid was based on the pressure from the nearest tap by tracing indices.

In order to estimate the area-averaged pressure for any given region, we partially adopted the method given by Dutithn et al. [16], and the modified method is explained here with respect to the presented building. Fig. 3 illustrates the adopted methodology, where each sub-figure represents the steps to calculate the area-averaged pressure for various zones. For square corner zones, Actions a, b and c should be followed, whereas for rectangular zones (such as edge zone and interior zone), Actions a, b and c should be followed first. Once all cells in least dimension of the target zone are selected, then Actions d and e need to be followed. The above procedure starts with the smallest cell matrix (i.e., 3 × 3 cell matrix with area of 9 ft^2 in this study). The detailed description for each action is given below:

i) Action a [Fig. 3(a)]: The procedure starts with a 3×3 cell matrix with an area of 9 ft^2. The matrix moves horizontally first with a step value of 1 cell unit until it reaches to the last cell matrix that has the same vertical coordinates in the target zone.

ii) Action b [Fig. 3(b)]: The 3×3 cell matrix moves in a vertical direction with a step value of 1 cell from the 1st column. Action a is repeated with the same size cell matrix. This process is repeated until the last corner cell of the selected zone is considered for calculation.

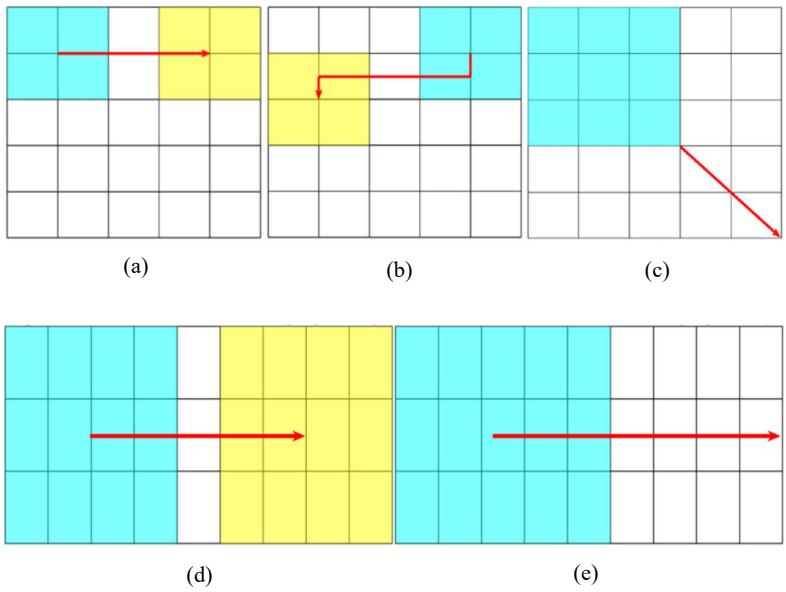

Fig. 3. Methodology in this study.

iii) Action c [Fig. 3(c)]: The size of the cell matrix is increased by adding 1 cell in each direction, resulting in an effective wind area of 16 ft^2. Actions a and b are then repeated with this larger matrix until all cells in the target zone are considered in calculation.

iv) Action d [Fig. 3(d)]: Once all cells in the least dimension of the selected rectangular zone are selected using Actions a, b, and c, the cell matrix moves in the direction of the larger dimension of the rectangular with the step value of 1 cell.

v) Action e [Fig. 3(e)]: Cell matrix moves in the direction of the larger dimension of the selected rectangular zone by a step value of 1 cell.

In addition, an envelope approach was adopted to account for extreme wind conditions, and the maximum area-averaged pressure was calculated for each effective wind area. In this study, the peak pressure was estimated as the 78^{th} percentile of the extreme value distribution using Liebein BLUE [19] method with 16 segments, as discussed in [18]. In the present study, gust effect factor (G) was estimated using the equation given by Wang & Kopp [22], which is based on the time domain perspective. This is in contrast to the equation adopted in ASCE 7-22, proposed by Solari [9][10], which is based on the frequency domain. Readers can refer to the mentioned references for more detailed information of gust effect factor equation.

3 Results and Discussions

In this section, we will present the results for various zones as defined in Section 2. We will examine the Gaussianity of C&C wind loads by presenting the skewness and kurtosis, which are the third and fourth order moments of statistical distributions. It is important to note that a skewness of zero and a kurtosis of three indicate a Gaussian distribution. Specially, Section 3.1 will provide the mean pressure coefficient distribution on the building roof, which will illustrate the complicated vortical structures over roofs. Sections 3.2 to 3.4 will present the gust effect factors of wind loads on different zones, along with the examination of skewness and kurtosis.

3.1 Mean Pressure Distribution on Roof

Figs. 4a and b depict the mean pressure coefficients obtained from the provided dataset for wind directions parallel and perpendicular to the building roof ridge, respectively. Meanwhile, Figs. 4c and d present the pressure distributions for oblique wind directions. For Figs. 4a and b, where wind is parallel and perpendicular to roof ridge, respectively, the high wind pressures are observed at the leading edge of the roof, with a gradual decrease in pressures as the tap location moves away from the leading edge in the along-wind direction. This behavior is mainly caused by the separated shear layer resulting from flow separation at the sharp-edge of roof. On the other hand, for oblique wind directions as shown in Figs. 4c and d, the large peak suction on the roof is accompanied by the development of a strong conical vortex on the roof [24]. The magnitude of the conical vortices reduces considerably along the wind direction, resulting in uneven pressure magnitude at the corner and interior zones of the roof. These complicated vortical structures may lead to wind pressures to follow non-Gaussian distribution, which will be examined in the following sections.

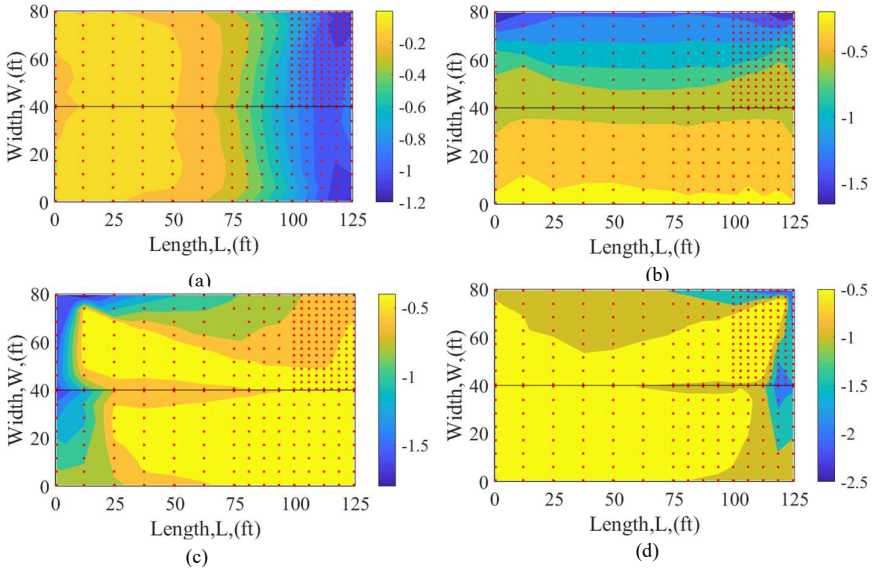

Fig. 4. Mean pressure coefficient distribution at roof: (a) Wind direction 360 °; (b) Wind direction 270 °; (c) Wind direction 225°; (d) Wind direction 315°

3.2 Corner Zone

Wu and Kopp [14] has indicated that estimating uplift fluctuations using QST is reasonable for large areas but would underestimate the fluctuations for small areas. Therefore, we will examine the relationship between statistical variables and gust effect factor and effective wind area. Due to the symmetry of this building configuration, we mainly focused on corner zone A-2 with high pressure tap density. Fig. 5 illustrates the gust effect factors for wind loads on corner zone A-2 as shown in Fig. 1. It is observed that the skewness is approximately -0.62, and the kurtosis is scattered around 3.54, respectively, as shown in Figs. 5a and b. This observation indicates that wind loads on corner zones do not follow a Gaussian distribution with a skewness of zero and kurtosis of three. As discussed in [24], conical vortices are the primary cause of peak wind pressures on roof corners. Therefore, we can conclude that these complex body-generated vortices change the statistical distribution of wind loads. Similar conclusions were also made in Wang and Kopp [22][25]. Additionally, the gust effect factors extend the recommended constant value of 0.85 for rigid structures in ASCE 7-22 due to the effects of conical vortices. The gust effect factors exhibit a slight decreasing trend with effective wind area starting from an effective wind area of 36 ft^2 as shown in Fig. 5c. In summary, we can make a conclusion that body-generated turbulence, such as conical vortices over building roof corners, results in wind loads following a non-Gaussian distribution and increases the gust effect factors associated with C&C wind loads.

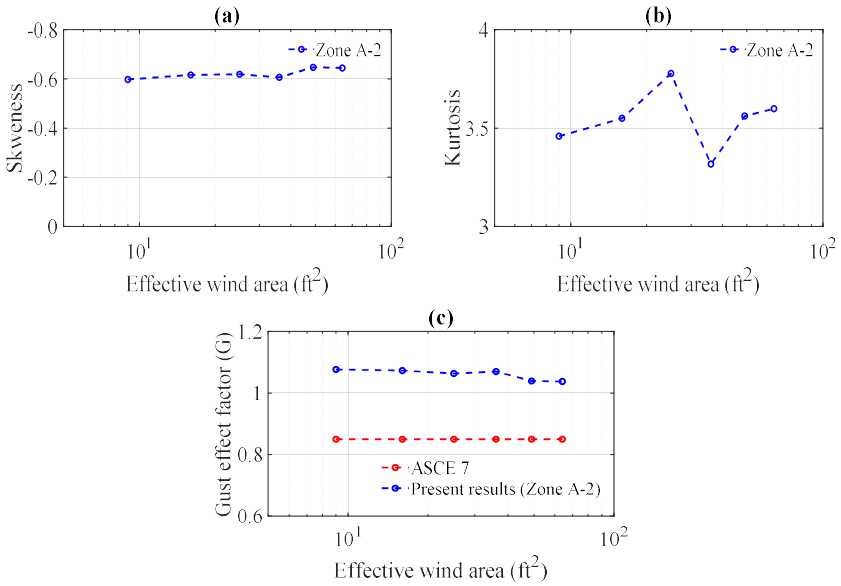

Fig. 5. Gust effect factors and statistics versus the effective wind area for Corner Zone A-2: (a) skewness; (b) kurtosis; (c) gust effect factor.

3.3 Edge Zone

Figs. 6 and 7 illustrate the results for edge zones B-1 and B-3, respectively. These two edge zones exhibit the most severe wind pressures at the given wind directions from 180º to 360º, as shown in Fig. 2. For Zone B-1, both skewness and kurtosis demonstrate a distinct dependence on effective wind area. Wind pressures are observed to follow a Gaussian distribution more closely for larger effective wind areas. This trend is also observed for gust effect factor, as depicted in Fig. 6c, and is similar to the peak wind pressure variation suggested in ASCE 7-22 and NBCC 2020. The reduced correlation/coherence of wind pressures on larger area may be the primary reason for the decreasing tendency with effective wind area. For effective wind area greater than 300 ft^2, the measured gust effect factor obtained from wind tunnel data approaches the recommended constant value of 0.85, implying that QST is applicable for larger areas. However, for smaller effective wind areas, the current gust effect factors based on wind tunnel data significantly exceed the recommended constant value of 0.85 in ASCE 7-22. The most significant underestimation could reach up to 23%. This finding is consistent with the discussion in Wu and Kopp [14] which suggests that QST is reasonable for evaluating uplift fluctuations for large areas while would underestimate the uplift fluctuation for small areas due to the neglect of body-generated turbulence in QST. For Zone B-3 as shown in Fig. 7, similar observations can be drawn as for Zone B-1, which will not be repeated for brevity.

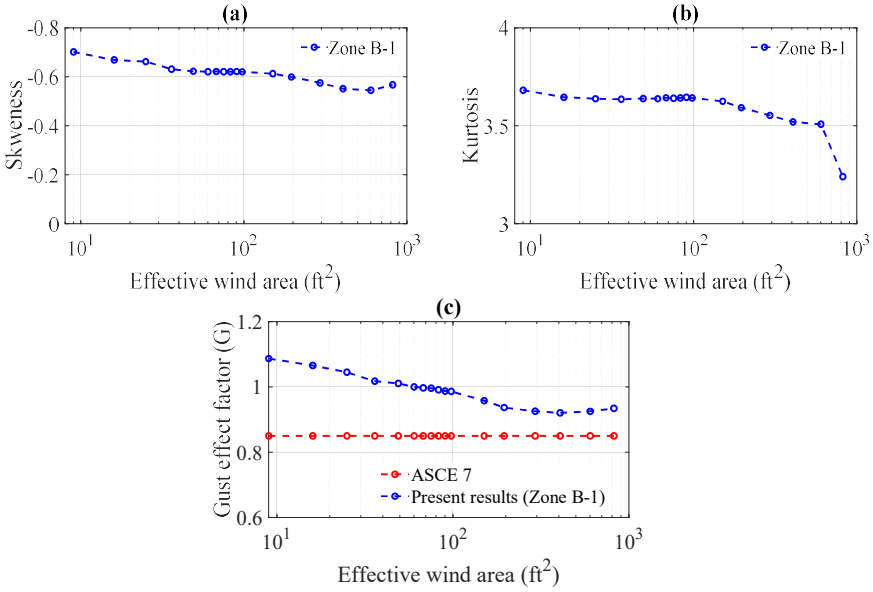

Fig. 6. Gust effect factors and statistics versus effective wind area for Edge Zone B-1: (a) skewness; (b) kurtosis; (c) gust effect factor.

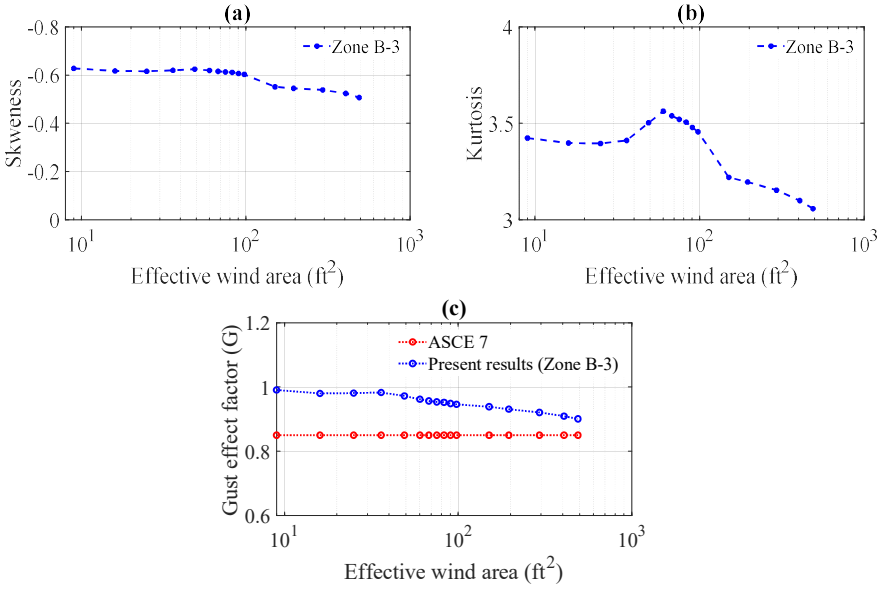

Fig. 7. Gust effect factors and statistics versus effective wind area for Edge Zone B-3: (a) skewness; (b) kurtosis; (c) gust effect factor.

3.4 Interior Zone

Fig. 8 displays the results for the interior Zone C. The statistical parameters and gust effect factors exhibit a similar performance as in the previous section for the edge zone. Wind loads on larger areas are observed to follow a Gaussian distribution more closely, as shown in Figs. 8a and b. An important observation worth noting is that the gust effect factor for effective wind areas greater than 1000 ft^2 approaches the constant value of 0.85 suggested in ASCE 7-22, indicating the QST holds for the large effective wind areas. This finding is consistent with Wu and Kopp's discussion that QST is reasonable for estimating wind pressure fluctuation for large roof area. The decreased gust effect factor for larger effective wind area is attributed to the reduced correlation/coherence of wind pressures over larger areas as well.

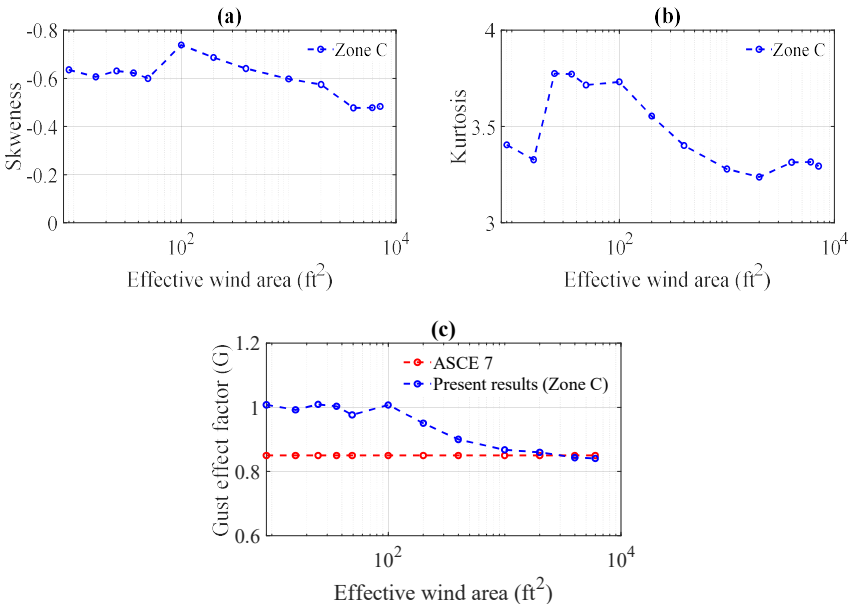

Fig. 8. Gust effect factors and statistics versus effective wind area for Interior Zone C: (a) skewness; (b) kurtosis; (c) gust effect factor.

4 Conclusions

This study aims to assess the applicability of gust effect factor method for predicting the C&C wind loads on one typical low-rise building roof using wind pressure data from the NIST aerodynamic database [15]. In order to illustrate the effects of body-generated turbulence on statistical features of wind loads, the skewness and kurtosis were examined in detail. This study defined three zone, namely corner zone, edge zone,

and interior zone, consistent with NBCC 2020. The conclusions of this study are summarized as follows:
1) A shear layer is formed by the flow separation at the sharp edge of the roof, and for oblique wind directions, conical vortices are generated around the roof corner, which are usually responsible for peak wind loads. These complex vortical structures change the statistical distribution of wind loads.
2) For the corner zone, non-Gaussian distributions of C&C wind loads are observed due to conical vortices, indicating that the QST is not applicable for corner zones with small effective wind areas. Neglecting body-generated turbulence effects, as ASCE 7-22 gust effect factor model does, would result in the underestimation of the measured gust effect factor.
3) For edge zone, the statistical characteristics of wind loads and gust effect factors show a decreasing tendency with effective wind area, which is similar to that for peak wind pressures suggested in ASCE 7-22 and NBCC 2020. The reduced correlation/coherence of wind pressures over large areas is considered as the main reason for the reduced gust effect factor.
4) For interior zone, the observations are similar to those for the edge zone. However, the gust effect factor for a large effective wind area greater than 1000 ft^2 is approaching the constant value of 0.85 suggested for rigid buildings in ASCE 7-22, indicating that QST holds for large effective wind areas. This finding is consistent with Wu and Kopp [14].

The primary objective of this study is to examine the applicability of the gust effect factor model in predicting C&C wind loads on building roofs that are notably affected by body-generated turbulence, such as separation bubbles and conical vortices. These complex flow patterns are fairly typical for low-sloped roofs. Therefore, we primarily focused on a typical low-sloped roof building configuration for open terrain in the NIST database. Choosing other low-sloped roof building configurations would not alter the conclusion that body-generated turbulence significantly affects gust effect factors in corner zones with small areas, whereas the effects are less significant for large areas in the internal zone, except for the gust effect factor magnitudes. However, further investigation is necessary for other terrains and more building configurations, which we intend to undertake in future studies.

5 Acknowledgement

The authors gratefully acknowledge Start-up Grant and WSS-Seed Grants awarded by University of Western Ontario, Canada.

6 References

[1] P. Krishna, “Wind loads on low rise buildings — A review,” J. Wind Engg. and Ind. Aero., vol. 54–55, pp. 383–396, February, 1995, doi: 10.1016/0167-6105(94)00055-I.

[2] Mehta, K., “Wind induced damage observations and their implications for design practice”, Engg. Struct., Volume 6, no. 4, pp. 242–247, October, 1984, doi: 10.1016/0141-0296(84)90019-1.
[3] S.-G. Yum, J.-M. Kim, and H.-H. Wei, “Development of vulnerability curves of buildings to windstorms using insurance data: An empirical study in South Korea,” Journal of Building Engineering, vol. 34, p. 101932–, 2021, doi: 10.1016/j.jobe.2020.101932.
[4] A.-M. Aly and J. Bresowar, “Aerodynamic mitigation of wind-induced uplift forces on low-rise buildings: A comparative study,” Journal of Building Engineering, vol. 5, pp. 267–276, 2016, doi: 10.1016/j.jobe.2016.01.007.
[5] G. A. Kopp and M. J. Morrison, “Component and Cladding Wind Loads for Low-Slope Roofs on Low-Rise Buildings,” J. Struct. Engg., vol. 144, no. 4, April, 2018, doi: 10.1061/(ASCE)ST.1943-541X.0001989.
[6] ASCE, “WIND LOADS: COMPONENTS AND CLADDING”, in Minimum Design Loads and Associated Criteria for Buildings and Other Structures. Reston, VA, USA, ASCE, 2022, pp. 315-350, doi.org/10.1061/9780784415788.
[7] CANADIAN COMMISION ON BUILDING AND FIRE CODES, “National Building Code of Canada – Volume 1”, Ottawa, ON, Canada, 2020, pp. 4-29 – 4-52, doi.org/10.4224/w324-hv93
[8] Davenport, A. G. "Gust loading factors." *Journal of the Structural Division*, vol. 93, no. 3, 1967.
[9] Solari G., “Gust buffeting. I: peak wind velocity and equivalent pressure”, J. Struct. Engg., vol. 119, no. 2, pp. 365-382, February, 1993, doi.org/10.1061/(ASCE)0733-9445(1993)119:2(365).
[10] Solari G., “Gust buffeting. II: dynamic along-wind response”, J. Struct. Engg., vol. 119, no. 2, pp. 383-398, February, 1993, doi.org/10.1061/(ASCE)0733-9445(1993)119:2(383).
[11] T. G. Stathopoulos, “Turbulent wind action on low rise buildings,” ProQuest Dissertations & Theses, Ann Arbor, 1979.
[12] Meecham, D., “Wind action on low-rise buildings.” M.E.Sc. thesis, Univ. of Western Ontario, London, ON, Canada, 1988.
[13] T. Stathopoulos, R. Marathe, and H. Wu, “Mean wind pressures on flat roof corners affected by parapets: field and wind tunnel studies,” Engg. Struct., vol. 21, no. 7, pp. 629–638, July, 1999, doi: 10.1016/S0141-0296(98)00011-X.
[14] Wu, C.H. and Kopp, G.A., 2018. A quasi-steady model to account for the effects of upstream turbulence characteristics on pressure fluctuations on a low-rise building. *Journal of Wind Engineering and Industrial Aerodynamics*, *179*, pp.338-357.
[15] T. C. E. Ho, D. Surry, D. Morrish, and G. A. Kopp, “The UWO contribution to the NIST aerodynamic database for wind loads on low buildings: Part 1. Archiving format and basic aerodynamic data,” J. Wind Engg. and Ind. Aero., vol. 93, no. 1, pp. 1–30, January, 2005, doi: 10.1016/j.jweia.2004.07.006.
[16] D. Duthinh, J. A. Main, M. L. Gierson, and B. M. Phillips, “Analysis of Wind Pressure Data on Components and Cladding of Low-Rise Buildings,” ASCE-ASME J. of risk and uncertainty in Engg. systems. Part A, Civil Engineering, vol. 4, no. 1, April, 2018, doi: 10.1061/AJRUA6.0000936.
[17] ASCE, “WIND LOADS: COMPONENTS AND CLADDING”, in Minimum Design Loads for Buildings and Other Structures. Reston, VA, USA, ASCE, 2010, pp. 257-297, doi.org/10.1061/9780784412916.
[18] E. Gavanski, K. R. Gurley, and G. A. Kopp, “Uncertainties in the Estimation of Local Peak Pressures on Low-Rise Buildings by Using the Gumbel Distribution Fitting Approach,” J. Struct. Engg., vol. 142, no. 11, November, 2016, doi: 10.1061/(ASCE)ST.1943-541X.0001556.

[19] Lieblein J., “Efficient methods of extreme-value methodology”, vol. 74–602. Gaithersburg, MD: U.S. Dept. of Commerce, National Institute of Standards and Technology, 1974.

[20] E. Gavanski, B. Kordi, G. A. Kopp, and P. J. Vickery, “Wind loads on roof sheathing of houses,” Journal of wind engineering and industrial aerodynamics, vol. 114, pp. 106–121, March 2013, doi: 10.1016/j.jweia.2012.12.011.

[21] L. M. S. Pierre, G. A. Kopp, D. Surry, and T. C. E. Ho, “The UWO contribution to the NIST aerodynamic database for wind loads on low buildings: Part 2. Comparison of data with wind load provisions,” Journal of wind engineering and industrial aerodynamics, vol. 93, no. 1, pp. 31–59, 2005, doi: 10.1016/j.jweia.2004.07.007.

[22] J. Wang and G. A. Kopp, “Gust effect factors for windward walls of rigid buildings with various aspect ratios,” J. Wind Engg. and Ind. Aero., vol. 212, p. 104603–, May, 2021, doi: 10.1016/j.jweia.2021.104603.

[23] H. W. Tieleman, “Wind tunnel simulation of wind loading on low-rise structures: a review,” Journal of wind engineering and industrial aerodynamics, vol. 91, no. 12, pp. 1627–1649, December, 2003, doi: 10.1016/j.jweia.2003.09.021.

[24] Kawai, H., 2002. Local peak pressure and conical vortex on building. Journal of Wind Engineering and Industrial Aerodynamics, 90(4-5), pp.251-263.

[25] J. Wang and G. A. Kopp, “Gust effect factors for regions of separated flow around rigid low-, mid-, and high-rise buildings,” J. Wind Engg. and Ind. Aero., vol. 232, p.105254, 2023, doi: https://doi.org/10.1016/j.jweia.2022.105254.